Cold Regions Science and Technology 211 (2023) 103844

Contents lists available at ScienceDirect

Cold Regions Science and Technology

journal homepage: www.elsevier.com/locate/coldregions

Can big data and random forests improve avalanche runout estimation compared to simple linear regression?

Håvard B. Toft [a,b,*], Karsten Müller [a,b], Jordy Hendrikx [c,e], Christian Jaedicke [d,e], Yves Bühler [f,g]

[a] Norwegian Water Resources and Energy Directorate, Oslo, Norway
[b] Department of Geosciences, University of Oslo, Oslo, Norway
[c] Antarctica New Zealand, Christchurch, New Zealand
[d] Norwegian Geotechnical Institute, Oslo, Norway
[e] UiT The Arctic University of Norway, Tromsø, Norway
[f] WSL Institute for Snow and Avalanche Research SLF, Davos Dorf, Switzerland
[g] Climate Change, Extremes and Natural Hazards in Alpine Regions Research Center CERC, Davos Dorf, Switzerland

ARTICLE INFO

Keywords:
Snow
Avalanche
Empirical-runout
Random forest
α-β model

ABSTRACT

Accurate prediction of snow avalanche runout-distances in a deterministic sense remains a challenge due to the complexity of all the physical properties involved. Therefore, in many locations including Norway, it has been common practice to define the runout distance using the angle from the starting point to the end of the runout zone (α-angle). We use a large dataset of avalanche events from Switzerland ($N = 18{,}737$) acquired using optical satellites to calculate the α-angle for each avalanche. The α-angles in our dataset are normally distributed with a mean of 33° and a standard deviation of 6.1°, which provides additional understanding and insights into α-angle distribution. Using a feature importance module in the Random Forest framework, we found the most important topographic parameter for predicting α-angles to be the average gradient from the release area to the β-point. Despite the large dataset and a modern machine learning (ML) method, we found the simple linear regression model to yield a higher performance than our ML attempts. This means that it is better to use a simple linear regression in an operational context.

1. Introduction

Snow avalanches, hereafter called avalanches, are a rapid flow of snow moving down-slope due to gravity. Avalanches release as a result of a number of factors including meteorological conditions, snow metamorphism and a triggering event. Several factors control the likelihood of an avalanche release, such as snowpack stratigraphy, slope steepness and aspect, precipitation rate, wind transported snow, air temperature, and vegetation. An avalanche has a start zone where the avalanche releases and accelerates, a track where the avalanche reaches its maximum speed and potentially entrains more snow and the runout zone where the snow decelerates and deposits. The transition between these zones can vary by avalanche path and size. The size of the resulting avalanche's track and runout zone are a function of the terrain and the volume of snow included in the avalanche event. Slab avalanches can occur wherever there is sufficient snow on the ground and a slope steep enough to slide. The systematic identification of starting zones has been restricted to slope angle (terrain between 30° and 50°, occasionally 60°) and vegetation (no forest) (Schweizer et al., 2003). While the location where the avalanche stops, i.e., the runout distance, can be estimated using a diverse range of numerical models (e.g., Bartelt et al., 2013; Christen et al., 2010; Volk and Kleemayr, 1999, Mergili et al., 2017), these models require estimates of a number of parameters, including the snowpack conditions, depth and area of release, and rely on assumptions on the friction and turbulence parameters.

Since the 1980s, several numerical models have been developed to simulate runout distance, flow height and velocity. These models are able to follow terrain features (e.g., bends in gullies) and provide additional understanding to the nature of the avalanche flow and resulting impacts, beyond solely estimating runout distance. Today, these models are frequently used as a tool for assessing mitigation measures (Håland et al., 2015). One of the most well-established models is the Rapid Mass Movement Simulation (RAMMS) from the WSL Institute for Snow and Avalanche Research (SLF), which is applied for legally

* Corresponding author at: Norwegian Water Resources and Energy Directorate, Oslo, Norway.
E-mail address: htla@nve.no (H.B. Toft).

https://doi.org/10.1016/j.coldregions.2023.103844
Received 4 April 2022; Received in revised form 29 March 2023; Accepted 31 March 2023
Available online 5 April 2023

binding hazard zonation in Switzerland and other countries (Bartelt et al., 2013; Christen et al., 2010, Rudolf-Miklau et al., 2015).

However, as noted above, a challenge with numerical models is that they are highly dependent on friction parameters and the initial volume (i.e., fracture depth and release area size). Friction parameters cannot be measured in real time for every event and need to be estimated based on a limited number of recalculations of known events or estimates of expected flow dynamics as a function of the snowpack conditions. The models are also highly sensitive for the release volume, hence the fracture depth and release area size in each scenario can be decisive for the results of the model run. The models are typically calibrated to known maximum runouts and each input parameter are calibrated to these events with respect to the runout distance.

Numerical models are also more challenging to apply across large spatial extents, though recent advances in computing power make this possible (e.g., Bühler et al., 2018; Harvey et al., 2018; Bühler et al., 2022). Therefore, due to these challenges, it has been common in Norway and some other countries to use a mathematical relationship as a first pass indication of possible maximum runout as a function of topographic parameters and climate, especially in the case of large-scale assessments (e.g., Larsen et al., 2020). This is commonly described as a statistical approach in snow avalanche literature, despite the fact that there is no explicit use of a statistical distribution. Oller et al. (2021) introduced the term empirical approach which is more accurate, and we will use this term in this paper.

When considering rapid gravitational flows, and not employing numerical models, it is common to use the angle of reach from horizontal (α) to define avalanche runout distance (e.g., Heim, 1932; Lied and Bakkehøi, 1980; Scheidegger, 1973). Using eq. 1 we can calculate the α-angle from the vertical distance H_α and the horizontal distance L_α. The distances are measured between the uppermost point of the release area and the lowermost point delimited by the avalanche debris (α-point) (Fig. 1). It is not explicitly stated whether we should use the straight-line length or the natural flow path (centerline) of the avalanche for L_α. We suspect, in practice, that most people have applied the α-angle using the straight-line approach. Therefore, we use the flow path when calculating the α-angle throughout this manuscript.

$$\alpha = arctan\left(\frac{H_\alpha}{L_\alpha}\right) \quad (1)$$

Empirical methods play an essential role in avalanche risk assessment and mapping and have been used as a baseline in most extreme avalanche runout scenarios worldwide (Oller et al., 2021). When assessing the characterization of avalanche runout models, there are two main approaches: (1) the α-β model and (2) the runout ratio model (McClung and Lied, 1987; Keylock, 2005). In this study we will focus on the α-β model developed by Lied and Bakkehøi (1980) as this model is commonly used in Norway. The α-β model relates the α-angle to a β_{10}-angle that represents the angle between the starting point and a β-point where the avalanche path reaches a slope incline of 10° (Fig. 1). The β_{10}-angle can be calculated by replacing H_α and L_α with H_β and L_β in eq. 1.

When the α-β method was applied to 285 avalanches in the French Alps, a valid β_{10}-angle was found within the avalanche in 79% of the avalanche events (Adjel, 1995), similar to 75% in Norway (Lied and Bakkehøi, 1980). Adjel (1995) also found that some avalanche events have several β_{10}-points; however, this is similar to what Lied and Bakkehøi (1980) documented in their data from Norway. Therefore, due to the dependency of the β_{10}-angle, the α-β method cannot be applied to all avalanche sites (Adjel, 1995; Lied and Bakkehøi, 1980).

Empirical approaches have been the focus of a number of studies over the last four decades, but all of them have been based on small datasets ranging from 30 to 216 samples (Oller et al., 2021). However, due to the low number of samples in each study, and variable method of path and event selection, these studies could be heavily biased as a function or a combination of the regional topography, or other unknown factors. Therefore, to understand empirical avalanche runout models more fully, and not solely for extreme events, we need to use a more extensive data set of avalanche events. Furthermore, given the limitations of the current α-β model, and its widespread use, there is a need for an updated model, based on this framework, that can be applied to all avalanche events, regardless of the presence of a β_{10}-angle. Both of these limitations can be addressed with a larger data set of avalanche events, and an updated analysis methodology of α-angles.

One method to obtain a more extensive data set is through remote sensing. In recent years, there has been tremendous progress in detecting avalanches using different remote sensing methods. One example is Malnes et al. (2015) which found a radar backscatter increase with avalanche debris. The increased backscatter could be identified using a change detection algorithm (Eckerstorfer et al., 2016, 2017, 2019). Another method is using optical imagery. Bühler et al. (2019) used SPOT6 imagery to manually delineate each avalanche event. Using

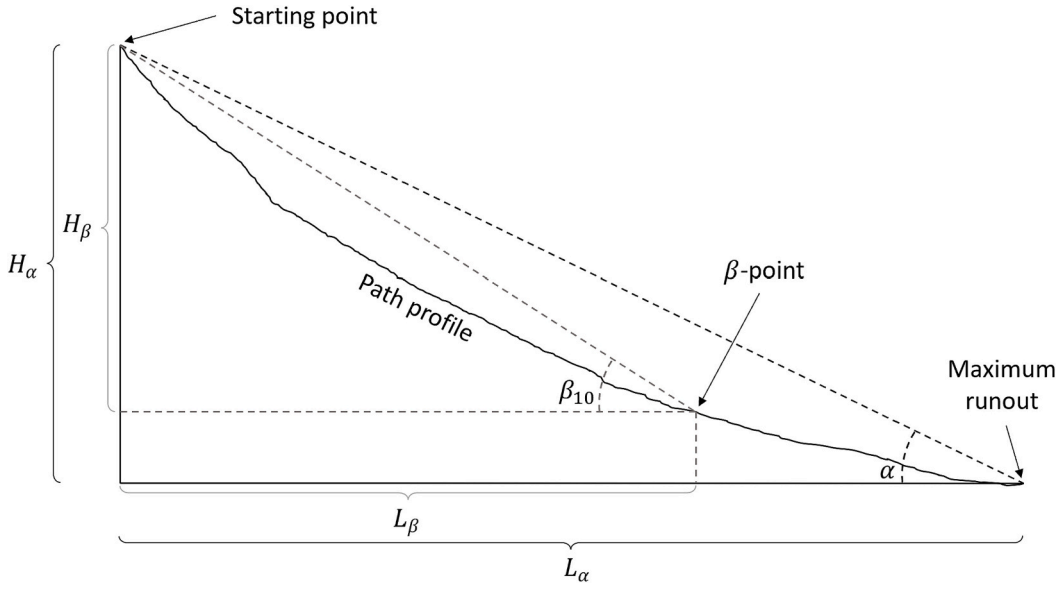

Fig. 1. The α-angle can be calculated when H_α and L_α are known, using eq. 1. These variables could be derived from a digital elevation model (DEM) when the starting point and α-point for an event are known. The same equation can be used to calculate the β_{10}-angle using H_β and L_β.

optical imagery, Bühler et al. (2019) were able to identify 18,737 avalanches ranging from size 1–5 (defined using area, Table 1) during an avalanche cycle in Switzerland in January 2018. Hafner et al. (2021) analyzed the quality of the satellite-based mapping and found it to be more accurate and complete than manual mapping. Utilizing these remotely sensed data from major parts of the Swiss Alps (Fig. 2), the number of samples is two orders of magnitude larger than the most extensive published dataset to date. These data can provide insights on how different topographic, snow-climate, and other parameters affect the runout distance, and provide us with the opportunity to reevaluate the current α-β model.

Therefore, we will focus on three linked research questions:

- Is it possible to determine the α-angle and associated topographic parameters from satellite observed avalanche events?
- How do topographic parameters influence the α-angle and resulting runout distance?
- Can we improve the prediction of α-angles for a larger range of avalanche events compared to previous studies using machine learning (ML) or linear regression?

2. Background

2.1. Empirical runout models

One of the big advantages of the empirical approach is that the inputs are relatively simple, static in time and not based on observed or modeled snowpack conditions. Starting with a dataset of 850 avalanche events, Lied and Bakkehøi (1980) calculated the α-angle for each event. We note that the term α-angle has been conflated with extreme events but is a parameter that can be estimated for any size event. Next, they removed the avalanches that didn't have a free outlet into the valley bottom, which left 423 avalanche events from 111 avalanche paths.

Finally, they performed a multiple regression analysis on the most extreme event from each of the 111 avalanche paths, using eight different terrain parameters. The β_{10}-angle resulted in the highest correlation compared to other features when only using one predictor (Eq. 2).

$$\alpha = 0.97\beta_{10} - 1.4^{\circ}(\pm 3.5^{\circ}) \quad (2)$$

Our study will expand on these methods, and apply them to our data set of 18,737 avalanche events, to explore if more data, from a different region provides different insights on the most important topographic parameters.

2.2. Machine learning

ML is a branch within artificial intelligence where statistics are used in combination with a computer to learn and make predictions from large amounts of data (Mohri et al., 2018). How much data is needed to make a good model depends on; (1) the complexity of the problem, and (2) the complexity of the ML algorithm. The physics describing the release and flow of avalanches are very complex and have only recently been simulated in 3D (Gaume et al., 2019; Li et al., 2021). However, these models require knowledge of the initial state of the snowpack prior to avalanche release. ML in combination with a large enough dataset can learn and approximate complex behavior based on relatively few input parameters. The drawback is that ML models act as black boxes not resolving why or how a certain input influences the model output. Lied and Bakkehøi (1980) found a simple linear regression model approach to provide the best balance between complexity and performance when developing the α-β model.

One commonly used ML algorithm is the Random Forest (RF). The algorithm work by training many decision trees on random subsets of the features, then averaging out their predictions. Such models composed of many other models are called ensembles: they are capable of boosting the performance of the underlying model (in this case, decision trees). Decision trees are versatile ML algorithms that can perform both classification and regression tasks, and even multioutput tasks (Geron, 2022).

When the sample sizes are sufficiently large, using RF, which is a nonlinear ML algorithm, is advantageous over a simple linear regression model as this approach can learn nonlinear relationships between input and output features. In addition, it is more flexible which means that it can estimate how many features are needed to make a good prediction and how important each input feature is. However, this added flexibility and capability comes at the cost of requiring a lot more data (number of samples). Previous avalanche datasets examining α-angles have been too small (i.e., 30 to 216 samples (Oller et al., 2021)), to fully leverage these more powerful ML methods. This study provides an opportunity to fully examine this more advanced methodology.

Table 1
Avalanche size as defined by Bühler et al. (2019).

Count	Size	Name	Area (m^2)
87	1	Small avalanche	10 to 500
5413	2	Medium avalanche	501 to 10,000
9863	3	Large avalanche	10,001 to 80,000
2857	4	Very large avalanche	80,001 to 500,000
157	5	Extremely large avalanche	> 500,000

3. Study area

All our remotely sensed avalanche data are from the Hafner and Bühler (2019) dataset, as presented in Bühler et al. (2019), which was collected after an avalanche cycle in January 2018 in Switzerland. The Swiss Alps cover 60% of Switzerland's total surface area, including the majority of the highest mountains in the European Alps, making it one of the world's most alpine countries. The study area within Switzerland consists of 12,500 km^2 stretching from the East to West of the Swiss Alps (Fig. 2). The south-eastern part of the Swiss Alps is not covered by the data set from Hafner and Bühler (2019) as it was not affected by extreme snowfall.

3.1. Description of the avalanche data

Bühler et al. (2019) tasked SPOT6 imagery after two large avalanche cycles in Switzerland on the 24th of January 2018. The 2017/2018 winter season started with a lot of snow across the Swiss Alps, including a recent snowfall event on the 5th of January. Then, from 8th through the 10th of January, southwestern Switzerland experienced an exceptional snowfall event of up to 200 cm of new snow reported in some areas. Further, between the 15th and 19th of January, another snowstorm with 30–100 cm, and in some areas up to 160 cm was reported. The snowstorm was associated with strong winds causing large amounts of snowdrift and resulted in the first cycle of extensive avalanche activity.

The second period from 21st to the 23rd of January was Switzerland's most extensive avalanche cycle since 1999 with another 60–150 cm of new snow above 2200 m. As a result, long-term snow measurement stations with 80-years of data observed record snow depths in many areas. The extreme avalanche cycle resulted in widespread avalanche activity including all avalanche sizes (Table 1) following 200–300 cm of new snow (locally, even more in the central Swiss Alps) over 15 days. SLF forecasted very high avalanche danger (level 5) three times during this 15-day period (Zweifel et al., 2019).

Each avalanche event was manually delineated using visual interpretation and GIS software. Contrast and brightness were tuned to improve the illuminated and shaded areas. Bühler et al. (2019) found that using a false-color band combination NIR (green, red, and near-infrared) made the snow avalanche debris stand more out. It made

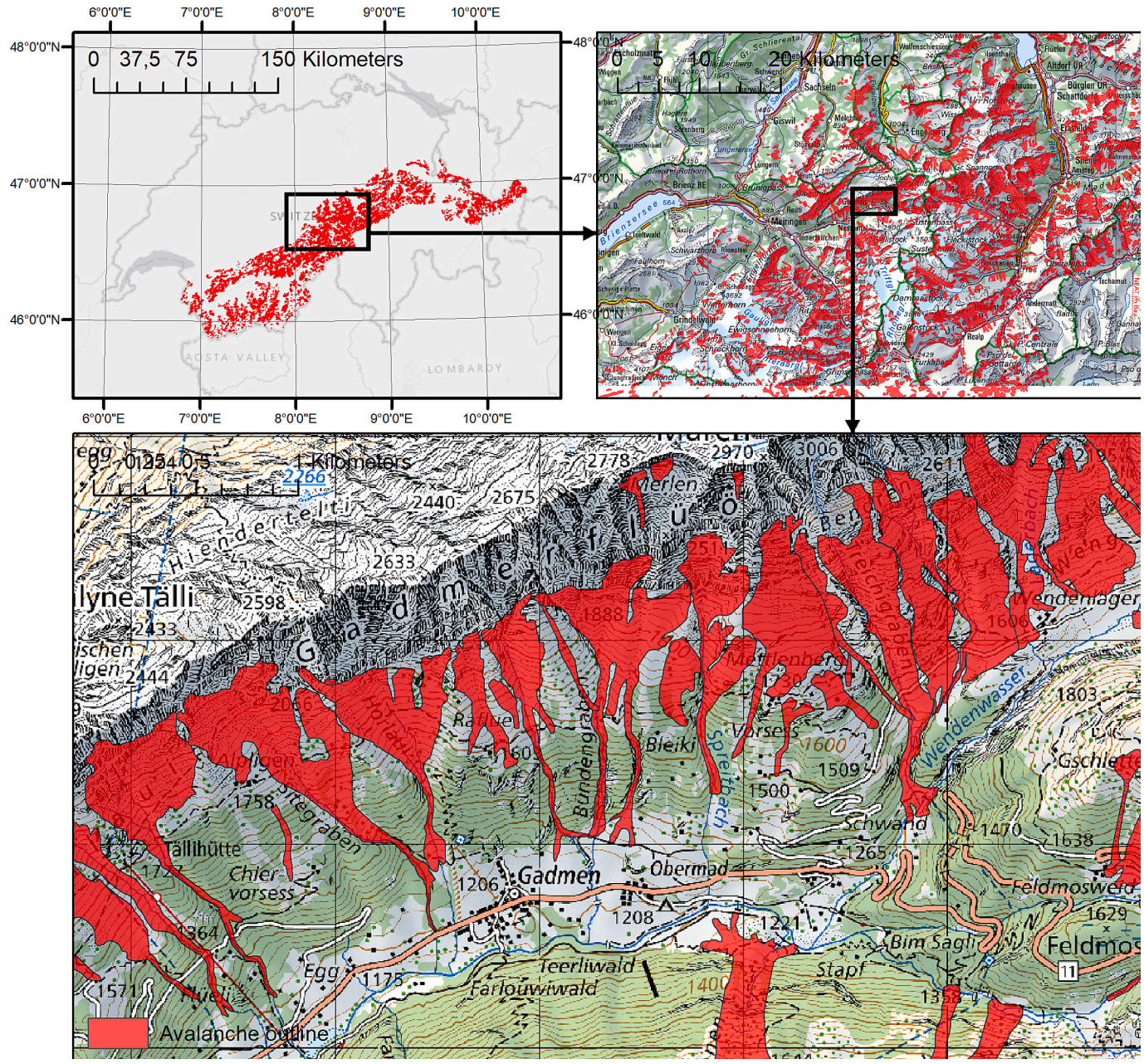

Fig. 2. The study area in Switzerland (upper left) and example of the avalanche data (Hafner and Bühler, 2019) at high resolution (red polygons in upper right and bottom maps, map source: Swiss Federal Office of Topography). (For interpretation of the references to color in this figure legend, the reader is referred to the web version of this article.)

forested areas more visible compared to a regular RGB image. Images were overlayed with an orthophoto and a slope angle layer of 30° at a scale of 1:5000. All avalanche events were mapped manually by one person.

In total, Bühler et al. (2019) mapped 18,737 avalanche events. The total area of all avalanches summed, was 936 km^2. Thus, making up 7.5% of the 12,500 km^2 large study area. They mapped 33% of the avalanche events with an exact outline, 58% had a partially estimated outline, while 9% of the avalanche events had the outline created by expert interpretation. Slab avalanches was the most common avalanche type at 72% of the mapped avalanche events, 11% where glide avalanches, and 3% where loose snow avalanches. The remaining avalanches are categorized as unknown. Bühler et al. (2019) divided their avalanche dataset into five classes (small, medium, large, very large, extreme) according to measured avalanche debris areas (Table 1).

4. Methods

Due to the large number of avalanche events analyzed in this analysis (N = 18,737), we developed an automated workflow using Python and GIS to extract topographic parameters for each individual avalanche event. We then applied a RF algorithm to create a model for variable importance and to predict avalanche runout length from the topographic parameters. All relevant Python code used can be found at GitHub (Toft, 2022).

4.1. Source data and parameters

The source data provided by Bühler et al. (2019) includes 18,737 polygons with additional metadata for each avalanche. We created two additional data formats to represent each avalanche event (Fig. 3).

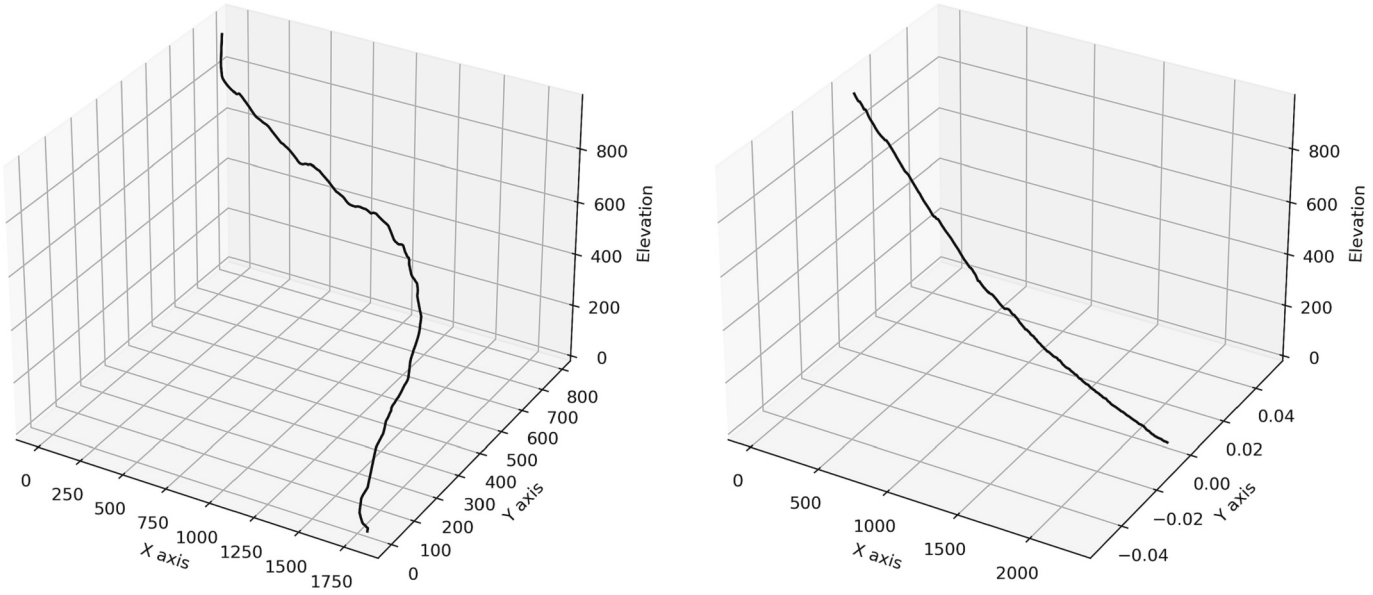

Fig. 3. Both figures represent the same avalanche path with reference number 5452. Left: A 3-dimensional centerline that represents the flow path through the avalanche from the starting point to the outermost point. Right: A 2-dimensional array of points where the z-axis is elevation, and the x-axis is the avalanche's horizontal length.

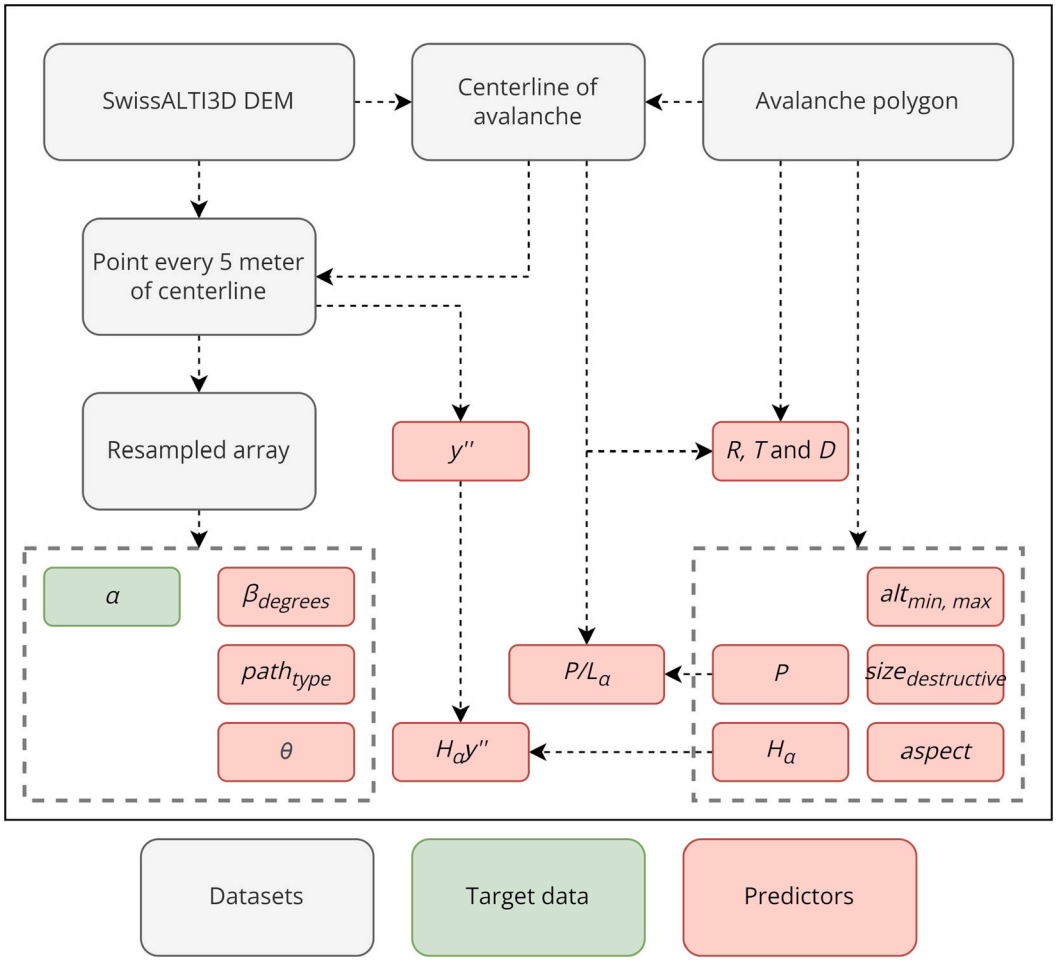

Fig. 4. Flowchart highlighting how each topographic parameter is derived from the DEM and avalanche polygons. Parameters are defined in Table 2.

To generate all the terrain-based metrics, the avalanches had to be within the extent of the Swisstopo swissALTI3D DEM (Swisstopo., 2018), resampled to a spatial resolution of 5 m (original data 2 m) to extract meaningful data. Reviewing the avalanche data from Hafner and Bühler (2019), we found that 79 avalanches were in adjacent countries which was outside the swissALTI3D DEM extent, leaving us with 18,658 avalanches for the analysis.

Using a combination of data from the DEM, avalanche polygons, polylines, and array, we defined all our metrics (Fig. 4, Table 2).

Our flowchart in Fig. 4 illustrates how we derived each topographic parameter from the original data.

4.1.1. Average gradient of avalanche flow path (α-angle)

The horizontal length (flow path) of the entire avalanche event (L_α) and the vertical elevation drop (H_α) are needed to calculate the α-angle. The known extent of the avalanche means that we can calculate the α-angle from the vertical and horizontal displacement using eq. 1. This is different from previous studies where the α-angles are measured with a clinometer in the field, or determined from a map with coarse contour lines (McClung and Lied, 1987).

4.1.2. Average gradient of avalanche track (β-angle)

The β-angle can be calculated when the horizontal length and vertical elevation change to the β-point are known (Fig. 1). To find the β-point, we fit a polynomial function to each flow path profile using a 2D array representing each avalanche event. Using this polynomial function, we use the derivative to find the intersection of β-point. We found a 7th degree polynomial to be the best representation of each avalanche profile (highest R^2). When the β-point is known, we can calculate the β-angle using eq. 1.

Some path profiles have several β-points. We resolve this by defining the β-angle as the first β-point after k, where k is the horizontal length of the avalanche in percentage from the starting zone (using a 7th degree polynomial fit to the avalanche profile). We examined multiple different $\beta_{degrees}$-angles. For $\beta_{5–15}$ we have defined $k = 50$, while for $\beta_{20–25}$ we have defined $k = 5$. If there is no valid β-angle, the path is assigned the value 0. Due to the size of the dataset, we had to apply an automated method for selecting an appropriate β-angle. The method presented above could differ slightly from the older studies, which were often based on manual profiling on topographic paper maps (i.e., Lied and Bakkehøi, 1980). However, the problem of selecting the correct β-angle is something that has been done in most studies, without defining a common way of doing it.

4.1.3. Inclination of starting zone (θ)

We have defined the inclination of starting zone as the angle between the upper release point and where the avalanche path drops below 30°. Using this threshold, we could use the same approach used in section 4.1.2, where we calculated the average gradient of the avalanche track. Using a threshold angle of 30° and $k = 5$, we can calculate each starting zone's average inclination (θ). We acknowledge that the selected definition is a simplification and may not fully capture the start zone inclination.

Table 2
Topographic parameters extracted from each avalanche used in the ML analysis. 33 predictors and 1 target in total.

Variable	Unit	Symbol
Average gradient of avalanche path	(°)	α
Average gradient of track	(°)	$\beta_{degrees}$
Inclination of starting zone	(°)	θ
Total vertical displacement	(m)	H_α
Elevation of deposits/release area	(m)	$alt_{min,\ max}$
Perimeter of avalanche	(m)	P
Profile of 2nd degree fitted polynomial path		y''
Profile of avalanche path described by path type		$path_{type}$
Minimum, maximum and mean width of rupture	(m)	$R_{min,\ max,\ mean}$
Minimum, maximum and mean width of track	(m)	$T_{min,\ max,\ mean}$
Minimum, maximum and mean width of deposit	(m)	$D_{min,\ max,\ mean}$
Aspect, 8 cardinal directions		$aspect$

4.1.4. Total vertical displacement

We calculated the vertical displacement (H_α) for each avalanche using the DEM. Using the tool, add surface information in ESRI ArcGIS, it is possible to calculate the highest (alt_{max}) and lowest (alt_{min}) point within a polygon. We did this for all avalanches. When exporting the attribute table to Python, and calculated H for each avalanche using eq. 3.

$$H_\alpha = alt_{max} - alt_{min} \tag{3}$$

4.1.5. Terrain profile of avalanche path

The shape of the avalanche path may potentially affect how the energy is dissipated on its way down the slope. A linear slope would cause no sudden energy loss, while an abrupt transition in the slope would. We applied two different approaches to examine this potential impact.

The first approach was using the radius of the path curvature as suggested by Lied and Bakkehøi (1980). The second derivative of a 2nd degree function is constant. The constant would express the type of curve of the 2D flow path of the avalanche. In our dataset, the value ranged from −0.03 to 0.06. A negative value means that the avalanche path is convex, while a positive value would mean that the avalanche path is concave. When the value is nearing zero, the shape is linear (or convex and concave terrain cancels each other out). Bakkehoi et al. (1983) found that if we assume that the slope is a parabola, we could derive the β-angle from the second derivative of y (y") and H_α using eq. 4.

$$tan\beta = \sqrt{\frac{H_\alpha y''}{2}} + \frac{tan10^\circ}{2} \tag{4}$$

To derive y", we performed a polynomial regression analysis for each avalanche path expressed as the equation $y = ax^2 + bx + c$. The mean R^2 was 0.993 with a standard deviation of 0.003. When a is known, we can use the relationship shown in eq. 5 to calculate y''.

$$y(x) = ax^2 + bx + c \rightarrow y''(x) = 2a \tag{5}$$

Our second approach used an unsupervised ML algorithm called K-Means clustering (Macqueen, 1967), which allows us to estimate the number of clusters in a dataset. Each cluster is categorical, and consists of a grouped set of data points due to their similarities. We used this algorithm to extract the most common avalanche path types ($path_{type}$). The algorithm was trained using a 2D array with 100 samples representing each avalanche event (Fig. 4). The centerline of each avalanche path is illustrated in Fig. 3. Here show and explain that we transform the 3D data into 2D data by flattening the y-axis. We then end up with a number of 2D coordinates representing the avalanche path. These coordinates are all resampled to 100 values per path, and used as input for the K-Means algorithm. We found the number of 8 clusters to be optimal based on visual inspection of the resulting clusters (Appendix, A-1).

4.1.6. Degree of confinement between starting zone and track

A large degree of confinement between the starting zone and the track could create higher avalanche velocities than unconfined slopes (Lied and Bakkehøi, 1980; Perla and Martinelli, 1976; Salm, 1972). Lied and Bakkehøi (1980) found the maximum width of rupture R_{max}, minimum width of the track T_{min}, and the maximum width of deposit D_{max} to be the most efficient way of incorporating the degree of confinement into a multiple regression analysis.

We calculated the length from the centerline to the polygon outline multiplied by two. We did this for every 5-m of the centerline. For this parameter, and recognizing that it is for the simplicity of the approach, we assume that the rupture area is the first 1/3 of the avalanche path

($R_{min,\ max,\ mean}$). The avalanche track is the second 1/3 of the avalanche ($T_{min,\ max,\ mean}$), while the deposit area is the last 1/3 of the avalanche path ($D_{min,\ max,\ mean}$). While this method oversimplifies the delineation of avalanche areas, it provides a simple and consistent method to capture the concept of avalanche path confinement. Bühler et al. (2013) used the same method to delineate release areas in their study. ML could be considered to help improve this predictor in future work.

4.1.7. Elevation of release and deposit area

We also included the value of the upper elevation of the release area (alt_{max}) and the value of the lowermost elevation of the avalanche deposits (alt_{min}) as a topographic parameter. These values are important, as an avalanche event that releases above treeline could have different properties than avalanches that release below, i.e., in the valleys.

4.1.8. Perimeter

The perimeter (or circumference) of each avalanche path polygon (P) in meters. The perimeter was extracted from the avalanche outline polygons.

4.1.9. Aspect

The aspect of each avalanche was provided in the dataset by Hafner and Bühler (2019). Each avalanche event aspect is defined using the eight cardinal wind directions (N, NE, E, SE, S, SW, W, and NW). We defined the cardinal wind directions to integers using the values 1–8 equivalently, where N was represented by 1 and NW by 8.

4.2. Methods to predict α-angles

Scikit-Learn is a Python module where a wide range of ML algorithms are made available to non-specialists in ML (Pedregosa et al., 2011). The module is easy to use, using a consistent interface that enables us to compare different ML methods without making significant changes to our code.

4.2.1. Linear regression

Linear regression is one of the simplest statistical models available in the Scikit-Learn library, and will be used as a baseline for the more advanced RF model. A linear regression analysis is used to predict a value using a linear relationship towards one other dependent feature. It's the same approach used by Lied and Bakkehøi (1980) when they suggested the α-β model.

4.2.2. Random Forest

RF is a well-documented ML method and is used in wide range of applications (Liu et al., 2012). RF is a supervised learning algorithm which means that it needs to know what the true answer is for each occasion. This is resolved by using two input data sets: (1) predictors and (2) target data. We use the topographic metrics as training data, while the α-angle is the target data (true reference value). Furthermore, the RF uses an ensemble learning method which means that it combines predictions from many different decision trees obtained by bootstrap to make the best possible prediction. The RF algorithm can be used with both categorical and continuous data. Because our target data is continuous, we use the RF regressor.

4.2.3. K-fold cross validation

In ML, it is common to split the data into test and training data. Training the model on the same samples used for validation would cause the model to repeat the pattern it had just seen, resulting in an overfitted model.

Cross-validation is a common method to avoid splitting the data into three groups (i.e., train, test, and validation) (James et al., 2013; Kuhn and Johnson, 2013). When using cross-validation, we train the model using *k-1* of the folds as training data. We use the remaining fold of the data for testing. When the algorithm finds the best parameters for the first model, the algorithm retrains the model using different *k-1* folds of the training data. When this iterative process is repeated k times, the model is fitted using all data as training data and test data.

There is no formal rule for selecting a value of k. James et al. (2013) and Kuhn and Johnson (2013) found that using $k = 5$ or $k = 10$ neither suffer from a high bias nor very high variance. In our models, we chose to use $k = 5$.

4.2.4. Feature importance

ML models, such as RF, are mostly used to predict a result. However, using the feature importance, it is also possible to measure which metrics that have the most effect on the model. Using this feature, we get the importance of each feature in percentage for a given model. As we want to find the optimal number of features, it is beneficial to learn how the model performs using selected features compared to all features.

4.2.5. Recursive feature elimination with cross-validation

Recursive feature elimination with cross-validation (RFECV) is a common way of removing features that are not important for the model (Guyon et al., 2002). It is reasonable to assume that some features are more important than others in predicting avalanche runout length. Therefore, we use RFECV to identify and remove unimportant features, intending to provide an improved model that is as parsimonious as possible, and therefore still relatively easy to apply for practitioners.

RFECV is a backward feature selection method that fits the model with all available features. The least important feature is then removed. This procedure is iterated until there is only one feature left in the model. Using RFECV we could find the optimal number of features (highest performing model), which makes it possible to create a simpler model while still being robust (Appendix A-2).

5. Results

5.1. The α-angle distribution

For our analysis we only considered avalanches with a calculated α-angle between 15 and 50°. All of these avalanche events outside of this range are outliers, and are suspected due to errors in our automated workflow. 27 avalanche events had an α-angle below 15°, and 264 avalanche events had an α-angle above 50°, which were removed. The

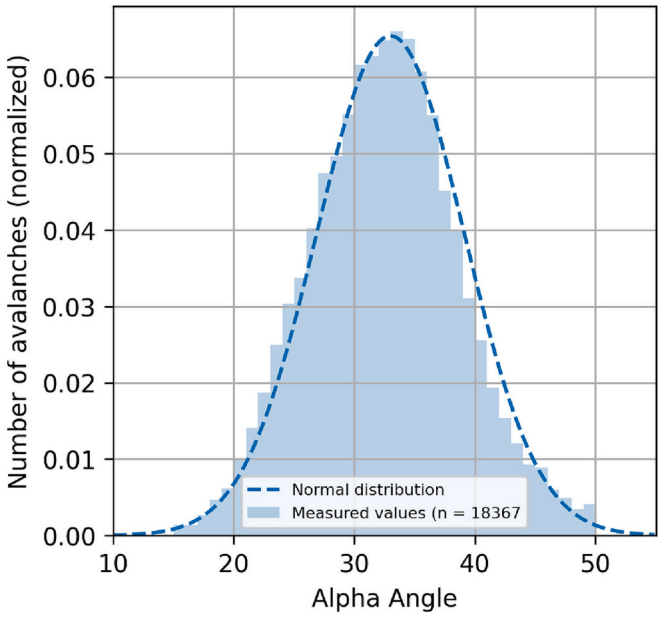

Fig. 5. The distribution of α-angles from the large avalanche cycle in Switzerland, January 2018.

final dataset used for training consists of 18,367 avalanches. We found the α-angles to have a mean of 33°, a median of 33° and a standard deviation of 6.1°. The α-angle distribution is plotted and compared to a normal distribution in Fig. 5.

5.2. Topographic features

We extracted 33 different metrics for 18,367 avalanches to be used as predictors (Table 3), while α is used as our target data (Table 4).

5.3. Feature importance

To find how important each feature is, we ran ten different RF regressors with 5-fold cross-validation using a different random state each time. When we use all 33 metrics as predictors, we can achieve an RMSE of 1.65 (± 0.31) (Fig. 6).

Reviewing the feature importance of the initial RF model using all 33 features as input, we found the β_{15} (63.0%), β_{25} (4.5%) and β_5 (4.0%) to be the three most powerful predictors (Table 3). The β-angles has a total summed feature importance of 84.29% The most important feature except the β-angles is the $H_\alpha y''$ with a feature importance of 4.0% (Table 3).

5.4. Predicting the α-angle

Unsurprisingly, the β-angles have the highest predicting power in terms of predicting the α-angle. Dividing the dataset into subgroups based on the type of β-angle therefore might yield information about what types of β-angles' are of most importance. Therefore, we chose to divide our dataset into subgroups. The lowest β_x available for each avalanche path is used to define each subgroup. Paths with a valid β_5 is in group 1, paths where the lowest valid β-angle is $\beta_{6–10}$ is in group 2, which similarly puts $\beta_{11–15}$ in group 3 and β_{16+} in group 4) (Fig. 7).

We also tried to divide the groups into smaller subgroups than 5° increments, which only improved the accuracy by a very small fraction (<0.01°).

We ran ten different RF regressors for each subgroup with 5-fold cross-validation. We used all 23–33 parameters as training data depending on the group. The accuracy metrics for each model are presented in Table 5. We see that the model from group 1 has the best accuracy with an RMSE of 1.43°, while group 2 has an RMSE of 1.52°, group 3 has an RMSE of 1.57°, and finally, group 4 has the lowest accuracy of all four models with an RMSE of 2.23°.

For group 1 and 2, which both have a valid β_{10}, it is also possible to use the standard α-β model framework. Using linear regression, we found the best α-β model for this dataset with RMSE of 2.40°, R^2 of 0.86 and a *p*-value of <0.01 (Eq. 6).

$$\alpha = 0.92\beta_{10} + 0.25^\circ (\pm 2.40^\circ) \quad (6)$$

The RMSE is substantially higher when using the standard α-β model framework, compared to our RF approach (Table 5). However, having 23–33 input parameters makes the model unwieldy, and essentially useless, from a practical standpoint.

5.4.1. Using RFECV to find optimal number of features

RFECV enables us to measure the performance of the model for a given number of features. It also enables us to remove features that are not informative. We apply the RFECV function to all of our four RF models and found that the best performance could be achieved with 27, 20, 10 and 4 features for group 1 through 4, respectively. However, nearly the same performance could be achieved with fewer features. To select the number of features in our models, we apply a threshold of improvement. If a model does not increase its performance by >10 % when another feature is added, we do not add this feature, and use the

Table 3
Descriptive statistics and feature importance of all the predictors used in the RF regressor.

Variable	N	Mean	Range	SD	5th percentile	25th percentile	50th percentile	75th percentile	95th percentile	Feature importance	Rank
aspect	18,367	–	–	–	–	–	N	–	–	0.2%	32
$path_{type}$	18,367	–	–	–	–	–	Type 3	–	–	0.5%	20
$size_{destructive}$	18,367	2.9	1–5	0.7	2	2	3	3	4	0.1%	33
P (m)	18,367	1209	49–19,423	1264	221	486	827	1451	3534	2.8%	5
alt_{min} (m)	18,367	2019	453–3981	507	1281	1637	1970	2374	2898	0.9%	15
alt_{max} (m)	18,367	2320	824–4457	476	1631	1972	2266	2636	3161	0.6%	18
β_5 (°)	8728	34	12–61	6	24	29	33	38	45	4.0%	3
β_6 (°)	9232	34	12–61	6	24	29	33	38	45	2.3%	6
β_7 (°)	9742	34	12–61	6	24	29	34	38	45	2.1%	7
β_8 (°)	10,267	34	12–60	6	24	30	34	38	45	1.3%	12
β_9 (°)	10,770	34	11–60	6	24	30	34	38	45	0.9%	16
β_{10} (°)	11,277	34	11–60	6	24	30	34	38	46	0.6%	17
β_{11} (°)	11,783	34	11–60	6	24	30	34	38	46	0.4%	23
β_{12} (°)	12,282	34	11–60	6	24	30	34	38	46	1.0%	14
β_{13} (°)	12,762	34	11–60	6	25	30	34	38	46	1.2%	13
β_{14} (°)	13,237	35	11–60	6	25	30	34	38	46	1.4%	10
β_{15} (°)	13,709	35	10–60	6	25	31	34	38	46	63.0%	1
β_{20} (°)	16,151	37	0–78	8	27	33	37	41	50	1.7%	9
β_{25} (°)	17,535	39	0–78	9	24	34	38	43	53	4.5%	2
θ (°)	17,970	40	0–79	10	22	35	41	46	56	1.3%	11
R_{mean} (m)	18,377	57	0–402	43	10	27	46	74	137	0.3%	29
R_{min} (m)	17,625	44	0–113	24	8	23	42	63	87	0.3%	24
R_{max} (m)	18,377	86	0–515	14	38	68	114	220	515	0.3%	30
T_{mean} (m)	18,377	74	0–507	62	11	30	57	98	194	0.3%	25
T_{min} (m)	17,401	60	0–499	51	9	24	46	81	157	0.4%	21
T_{max} (m)	18,376	94	0–517	14	39	73	124	250	517	0.3%	27
D_{mean} (m)	18,377	48	0–387	39	8	22	38	62	123	0.3%	28
D_{min} (m)	17,137	40	0–119	22	8	22	37	56	78	0.4%	22
D_{max} (m)	18,357	76	0–516	64	12	32	59	100	199	0.2%	31
H_α (m)	18,377	303	8.83–2674	249	66	133	224	389	811	0.3%	26
P/L_α	18,377	2.41	1.8–9.3	0.5	2.0	2.1	2.3	2.5	3.3	0.5%	19
$y'' (10^{-3})$	18,377	2.17	−31.2–68.3	3.2	−0.2	0.5	1.4	2.8	7.6	1.9%	8
$H_\alpha y''$ (m)	18,377	0.38	−2.6–4.2	0.4	−0.1	0.2	0.3	0.5	1.1	4.0%	4

Table 4
Descriptive statistics for the potential target data, where α_{flow} is the only one being used.

Variable	N	Mean	Range	SD	5th percentile	25th percentile	50th percentile	75th percentile	95th percentile
α (°)	18,367	33	15–50	6	22	28	33	37	43

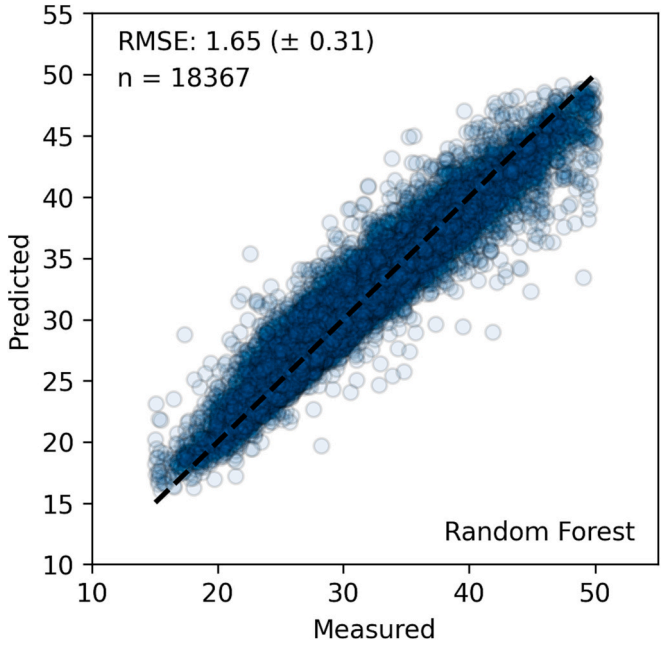

Fig. 6. A scatter plot showing the predicted α-angles vs. the measured α-angles for all 18,367 avalanches.

initial number of selected features. Using the threshold of improvement rule, we found the best number of features to be 1, 1, 1, and 3 for groups 1–4 respectively. The RFECV plots can be found in the Appendix (A-2).

When we apply the rule of improvement, the metrics are only a small fraction lower than the previous models using all 33 features as input. The accuracy metrics for each model is presented in Table 6. We see that group 1 has the best accuracy with an RMSE of 2.41°. Group 2 has an RMSE of 2.40°. Group 3 has an RMSE of 2.22°. Finally, group 4 has the lowest accuracy of all four models with an RMSE of 3.19°. We also present the results from a linear regression model for group 1–3. Here we see that the linear regression model outperforms the RF model with a RMSE of 2.01° for group 1 ($\alpha = 0.95\beta_5 + 0.06$), 1.99° for group 2 ($\alpha = 0.93\beta_{10} + 0.29$) and 1.84° for group 3 ($\alpha = 0.88\beta_{15} + 2.18$). Group 4 has >1 target features and is thus not compatible for the simple linear regression model. A scatter plot for each model can be found in the Appendix (A-3).

Table 5
The performance of the different RF models is compared using RMSE.

Categorization	RMSE	N / %	Training feature(s)	Number of features
All data	1.65° (± 0.31°)	18,367 / 100%	Table 3	33
Group 1	1.43° (± 0.31°)	8728 / 47.5%	Table 3	33
Group 2	1.52° (± 0.34°)	2555 / 13.9%	Table 3 – β_5	32
Group 3	1.57° (± 0.16°)	2511 / 13.7%	Table 3 – β_{5-9}	28
Group 4	2.23° (± 0.52°)	4573 / 24.9%	Table 3 – β_{5-14}	23
α-β model (Eq. 6)	2.40°	11,277 / 61.73%	β_{10}	1

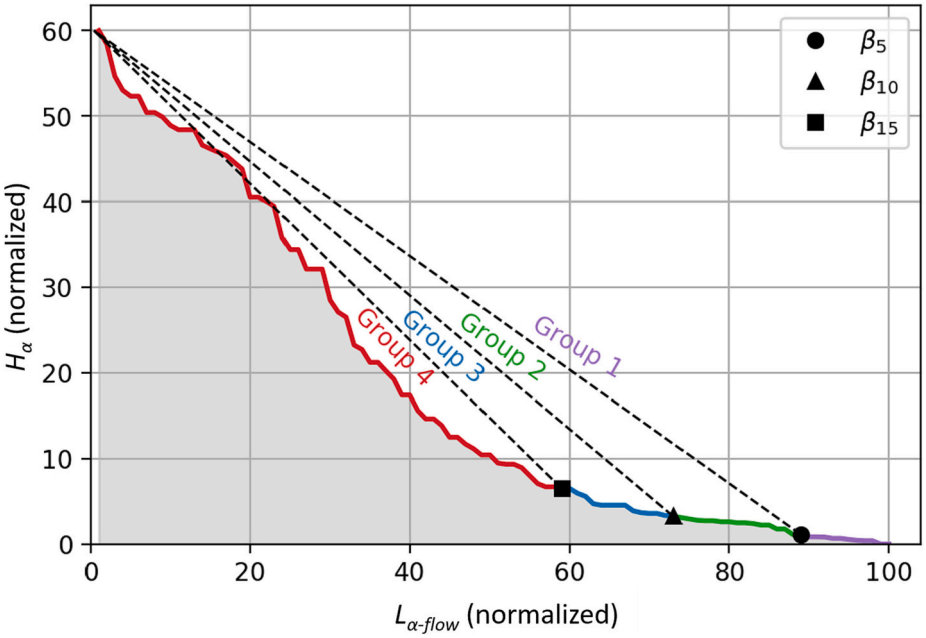

Fig. 7. The dataset is split into four groups using β_5, β_{10} and β_{15} as thresholds. The dashed line marks the intersection between each group. The colors mark the location in the avalanche path where the avalanche deposits stop. The normalized axis' range from 0 to 100. If L_α was 1700 m, its normalized to a range of 100, meaning that each full integer value represents 17 m. The same applies to the y-axis, see resampled array in Fig. 4.

Table 6
The performance of the different RF models is compared using RMSE. N is the number of samples; percent is the group size compared to the sample with all 33 features. The remaining features is the optimal number of features selected for the group model.

Categorization	Model	RMSE	N / %	Target feature(s)
Group 1	Random Forest	2.41° (± 0.27°)	8728 / 47.5%	β_5
	Linear Regression	2.01°		
Group 2	Random Forest	2.40° (± 0.39°)	2555 / 13.9%	β_{10}
	Linear Regression	1.99°		
Group 3	Random Forest	2.22° (± 0.18°)	2511 / 13.7%	β_{15}
	Linear Regression	1.84°		
Group 4	Random Forest	3.19° (± 0.36°)	4573 / 24.9%	$H_\alpha y''$, β_{25}, P
	Linear Regression	N/A		

6. Discussion

6.1. Definition of the α-angle

An issue with the definition of the α-angle (Lied and Bakkehøi, 1980) is that it does not always make sense to measure the length between the highest and lowest point of the avalanche, instead we must ensure that it is always measured in accordance with the avalanche flow path. An example to illustrate this issue can be seen in avalanche number 2022 with an incorrectly assessed α-angle of 8° (Appendix A-4). The avalanche was 1000 m wide and only 200 m long. The avalanche's highest point was on the west side, while the lowest point of debris was on the east side. The calculated flow path, which according to our automated workflow would be represented as a line connecting these points, resulting in an impossible flow path almost parallel to the slope's inclination (Appendix A-4). We, therefore, propose the following addition to the definition of the α-angle to clarify type of flow path and avoid confusion (*in italics*):

"$\alpha = arctan\left(\frac{H_\alpha}{L_\alpha}\right)$, where H_α is vertical height and L_α is total horizontal displacement. Measured between the highest point of release and the outer end of the avalanche deposit from any avalanche event *measured along the natural flow path of the avalanche.*"

In practice, we suspect that most people have applied the α-angle in this approach, using the natural flow path, but it is not explicitly stated, so we feel that this proposed addition reduces any potential ambiguity on this issue.

6.2. α-angle distribution

One of our main objectives was to find the α-angle distribution for all avalanche events using this historic avalanche cycle in Switzerland. Prior work in North America and the Alps only investigate large or extreme avalanche events. Lied and Bakkehøi (1980) are the only previous study to our knowledge that have mapped avalanche events of all destructive sizes, but having a much smaller data set ($N = 423$). Our α-angles are a representation of all avalanche events for the given study area during this cycle. They do not necessarily capture the historically longest observed run out in these paths. We believe that there is a common misconception that people conflate α-angles with extreme avalanche runouts. An α-angle is not exclusively reserved for the most extreme event, they simply represent the angle from the upper release point to the deposits of a given avalanche, following the natural flow path, which does not explicitly connect to return period or maximum size. However, we do acknowledge, and consider it likely that this is the cause for the confusion, that a common application of an α-angle is to determine the runout distance of low frequency events for hazard management and planning.

After the removal of outlier avalanche events outside the α-angle range of 15–50° our resultant data set decreased from 18,658 samples to 18,367 (roughly 0.15% of the samples were removed). The resulting α-angle range is similar to the 18–50° range that Lied and Bakkehøi (1980) found in their dataset. The mean of 33° is identical to the 33° mean which Lied and Bakkehøi (1980) found in their dataset when reviewing all their 423 avalanches in Norway. We also found a standard deviation of 6.1° compared to 6.3° for Lied and Bakkehøi (1980). The mean and standard deviation suggest that the distributions in Switzerland and western Norway are nearly identical when considering all avalanches, rather than exclusively focusing on the most extreme events.

It should be noted that Bühler et al. (2019), collected the Swiss dataset used in this study during extreme avalanche hazard (danger level 5) in January 2018. Therefore, we assume that most of the avalanches in the dataset are likely to be large or extremely large using the relative avalanche size scale (i.e., R4-R5 events), but for the entire range of destructive sizes (i.e., not just D4-D5 events). Based on the avalanche perimeters ranging from 50 to 20,000 m in our data we can assume that avalanches of all destructive sizes are represented. This could be investigated by historical studies or by numerical simulations with some standard parameters for all avalanche paths. One could then relate the observed avalanche to the modeled one and check for a relative size, however, this was considered outside the scope of the current work presented here.

6.3. Topographic parameters

One of our objectives was to develop automated methods for extracting the same topographic parameters that Lied and Bakkehøi (1980) used in their multiple regression model (Table 2) and investigate whether we could improve the α-β model. Utilizing a dataset with two orders of magnitude more data, we discovered that a simple linear regression still has the highest performance compared to the more modern RF algorithm.

6.3.1. β-angle

There are only limited studies that have examined different values for the β-point. McKittrick and Brown (1993) used a β-point of 18° for 24 avalanche paths in southwestern Montana. Using the original β-point of 10° would have been valid for only 20.83% of their avalanche paths. Another study is the estimation for short slopes done by Jones and Jamieson (2004) where they use a β-point of 24°. We, therefore, calculated different β-angles using different threshold angles for the β-point. We believe that the relation between different β-angles could provide critical input to the RF model.

Reviewing the feature importance, we were able to measure the significance of each topographic parameter. Our results support Lied and Bakkehøi (1980) findings, which found the β-angle to be the most important feature, with a total summed feature importance of 84.29%. We always found the lowest β-angle to be the most important factor for avalanches with a valid β-angle of β_{15} or lower. A prerequisite for this was that the given β-angle was available for all avalanches in the dataset. For example, with only valid β-angle of 6–10°, the β_{10} would be the most important because all avalanches in the dataset have this angle. This makes sense as the lower the β-angle, the closer the β-point is to the true α-point.

Another important issue in defining the β-point is the choice and resolution of the DEM for the study. Newer datasets based on high resolution laser data give more detail in the terrain, often leading to multiple beta angles as the resolution of the DEM increases. The original α-β model was developed based on 20 m isolines, not on gridded DEM data.

The choice of a 5 m grid and the rule to choose the lowest of multiple β-points might influence the results but was considered outside the scope of this current work.

6.3.2. $H_\alpha y''$

From the feature importance, we found $H_\alpha y''$ to be the second most important parameter after the β-angle with feature importance of 4.0%. Lied and Bakkehøi (1980) got the same result, thus not significant. If we assume that each avalanche follows a parabolic path, then the $H_\alpha y''$ is correlated with the β-angle (Bakkehoi et al., 1983). One considerable disadvantage with this parameter is that it is impossible to measure/assess in the field without various assumptions. Neither H_α nor y'' can be computed explicitly without knowing the whole avalanche path, meaning that we would have to make some assumptions to predict avalanche runout. Neither H_α nor y'' had any significance on their own. Because of this, model 4 which uses H_α and y'' inherit a higher uncertainty.

6.3.3. Avalanche size

Given the close relationship between avalanche size and avalanche danger in avalanche forecasting, we assumed that there would be a relationship between the α-angle and avalanche size. However, after reviewing the feature importance results, we found avalanche size to be negligible (0.16%), supporting Gauer et al. (2010), which found neither H_α nor volume dependency for avalanche runout distance. Plotting the α-angle for each avalanche versus destructive avalanche size, we find a small tendency towards larger avalanches produce longer runout distances (and lower α-angles). The tendency is as expected, but we hypothesized that it to be more pronounced than what we found in our data set. Our measure of avalanche size is only based on area. We have no means to derive the total volume or even the destructive potential used to classify destructive size (American Avalanche Association, 2016; Canadian Avalanche Association, 2016). Thus, our relationship might not represent the complete relationship between avalanche size and α-angle. Given the sample size of our dataset, we believe it to be close to the real correlation. However, we do not explicitly address the case of different sized events in the same avalanche path. In that scenario, we would still expect an R1 vs. an R5 avalanche from the same path to have very different α-angles.

6.3.4. Other parameters

Compared to the β-angles (84.29%) and $H_\alpha y''$ (4.0%), there are no other topographic parameters of significance. The P (2.8%), y'' (1.9%) and alt_{min} (0.9%) were the third, fourth and fifth most important parameters.

6.4. Model performance

6.4.1. Model performance using selected features

When we run RFECV, we find the optimal number of features in terms of maximum performance. The optimal number of features might not be the best with regard to ease of use by practitioners. For the model to be easy to use, we want to have as few input features as possible. Ideally, input parameters are easy to assess in the field. We resolved this by using a percentage threshold. To our knowledge, we have not seen this method being used to limit the number of features. The 10% threshold was set using our judgment of what we believed made sense and does build on similar concepts (i.e., the one standard deviation rule by Breiman et al. (1984)). The threshold reduced the number of optimal features significantly for all of our models.

After reducing the number of features, we still found the β-angle to be the most important feature for all models. The model from group 3 had the best ability to predict accurate results. This was surprising as we had expected the β_5-angles which are the closest to the maximum runout to yield the best performance.

If the higher valid β-angle yields lower accuracy, we should expect β_6 to be the most important parameter in model 2. This is not the case because β_6 is not valid for all avalanches in the group. β_{6-10} is given, but only β_{10} is valid for all avalanches. It is always the lowest β-angle that provides the most robust predictions, but it must apply to all avalanches to be useful for the group. Because of this, β_5 is the most important feature for group 1, β_{10} is the most important for group 2 and β_{15} is the most important for group 3.

There is a considerable disadvantage in using model 4. The model is more complex using 3 input features. The models also depend on $H_\alpha y''$. Both H_α and y'' rely on knowing the whole avalanche profile in advance, something we do not know when predicting avalanche runout. The unknown avalanche profile, combined with the much lower performance for these models, makes us not recommend using them. Model 4 would therefore not be relevant for hazard mapping and long runouts because high β-values limit both models. The high β-values mean that there are probably avalanches with a longer return period and a shorter runout, which are not a primary concern when making hazard maps and mapping long avalanche runouts.

6.4.2. Model performance compared with the simple linear regression

Initially, with all input parameters, the RF yielded better results than the simple linear regression. However, the numerous input parameters are nearly impossible for practitioners to apply in retrospect. We, therefore, applied RFECV and feature selection to reduce the complexity of the model. We found that the best balance between complexity and simplicity was by using one β-angle as input for model 1–3. The single input parameter makes it possible to compare the two different models with the same inputs. Using RMSE as a measurement of performance, we found the simple linear regression model to outperform the trimmed RF model. The simple linear regression model is also easier to apply by practitioners due to the output being a simple equation.

Another consideration for the relatively poor performance in the RF models is the degree of correlation between the variables. Appendix A-5 provides a correlation matrix for all the variables, which clearly shows the extent of the variable correlations. This has been demonstrated to impact the strength of predictors in other applications, which in turn, can influence overall model performance (Darst et al., 2018).

6.4.3. Deterministic versus probabilistic prediction

The α-β model is a deterministic prediction of the extreme runout to be expected in a given path (Eckert et al., 2008). The uncertainty considerations are only related to sample size and not a probability distribution. By contrast, other approaches exist, such as the runout ratio (McClung and Lied, 1987). The runout ratio uses a direct fitting of a probability distribution which means that it is possible to assess the likelihood of a certain runout length within a given path (more than one answer). The empirical relationship between runout distance and topography is the only similarity between the α-β model approach and the fitting of a distribution to the runout ratio model. We should therefore not interpret these two model types in the same way.

6.5. Limitations and future work

A limitation with our study largely inspired by the α-β model is that we are trying to make a model that outputs one single prediction for each avalanche path. In reality, it is possible with many different runout lengths for a single avalanche path. Lied and Bakkehøi (1980) solved this by choosing the most extreme avalanches in each path. Our RF method is similar, but we do not have the detailed information about whether the avalanches are the most extreme possible or not. We attempted to get around this by sorting our dataset into groups depending on where each avalanche stops in the path. The lack of detailed information about each avalanche means that it could be a natural variability within each group instead of a mean prediction plus an uncertainty like the results from Lied and Bakkehøi (1980). The improved performance of each group illustrates that having one single deterministic prediction of the runout

distance as a function of topography falls short of a probabilistic approach.

One of the advantages of our work is the large data set we could use to train and test our models. Our data includes many samples across an area of 12,500 km^2 from an extreme avalanche period over 15 days. Therefore, we believe that most of them are large to extreme size for their path, but we have no local knowledge of each avalanche event to confirm this. The lack of control of each avalanche event makes it challenging to know with a high degree of certainty what kind of avalanche events our model is good at predicting. When we consider the work by Lied and Bakkehøi (1980), they had excellent control of their avalanche events, selecting representative samples of avalanche events with the most extreme runout in each path. Local knowledge about each avalanche is more important for small data sets where outliers will have a larger impact on the analysis. Such a selection of events could also cause a bias in the dataset.

Another limitation is that because the β-angle is the only predictor, the parameter is scale independent. One given avalanche slope could have several different avalanche runouts which would yield different α-angles. In contrast, the topography remains constant, and thus the β-angle remains constant. This means that the model cannot reveal scale effects in runout distances which are definitely present in extreme runout data (McClung, 2022).

Future work could validate the model against avalanches in other regions outside of Switzerland. The validation could be done using real case studies and comparing the model against other numerical models such as RAMMS, Elba+, r.avaflow and the α-β model as done by Håland et al. (2015) and Oller et al. (2021).

Further investigations could consider the merits of ML algorithms or neural networks to improve the results compared to a simple regression model. The model could also be adjusted so that it's optimized for long runouts, i.e. the most extreme events, where incorrect assessments have the potential for the greatest impact. It would also be of interest if other datasets such as the Swiss dataset became available for other regions or climates. This would enable us to compare whether the overall α-angle distribution is different in other climates.

7. Conclusion

We use a large data set of over 18,000 avalanche events from Switzerland acquired using optical satellites to calculate the average gradient of avalanche flow path (α-angle). Using GIS methods, we have derived several topographic metrics for each avalanche event. We considered all events from a large avalanche cycle and did not focus solely on the most extreme events.

We developed methods to extract geometrical features from the avalanche polygons that are useful for statistics of avalanche events and model development or refinement. Given the increased availability of remote sensing data over the last decade we can expect to see more collections as provided by Hafner and Bühler (2019). Thus, our methods might aid in future analysis and comparison of e.g., mapped extreme avalanche cycles.

We found that, when we use α-angle as a proxy for avalanche runout length for all these events, we can summarize the data as a normal distribution with a mean of 33° and a standard deviation of 6.1°. The horizontal length of the α-angle should be measured using the natural flow path of the avalanche. We also re-iterate that an α-angle is simply the angle of reach from the top to bottom for any event, and we should not conflate it with only extreme events.

Using the feature importance in a RF, we found that the most important topographic parameter for predicting α-angle is the average gradient from the release area to the β-point (β_5, β_{10}, β_{15}). Other topographic parameters reviewed were not of any significance compared to the β-angles.

We explored a large dataset using a multitude of topographic parameters using the RF algorithm, which is one example of a modern ML algorithm. Despite this, we found the simple linear regression model to yield the highest performance. Furthermore, we refine the application of the α-β model by grouping the avalanches, showcasing that the selection of the β-point is important.

Our analysis provides additional understanding and insights into α-angle distribution, and the topographic controls thereof, across a range of avalanche sizes regardless of a valid β-point.

CRediT authorship contribution statement

Håvard B. Toft: Conceptualization, Investigation, Methodology, Software, Validation, Visualization, Writing – original draft, Writing – review & editing. **Karsten Müller:** Conceptualization, Writing – review & editing, Supervision. **Jordy Hendrikx:** Conceptualization, Writing – review & editing, Supervision. **Christian Jaedicke:** Writing – review & editing. **Yves Bühler:** Writing – review & editing.

Declaration of Competing Interest

The authors declare that they have no known competing financial interests or personal relationships that could have appeared to influence the work reported in this paper.

Data availability

Data available at GitHub.

Appendix A. Appendix

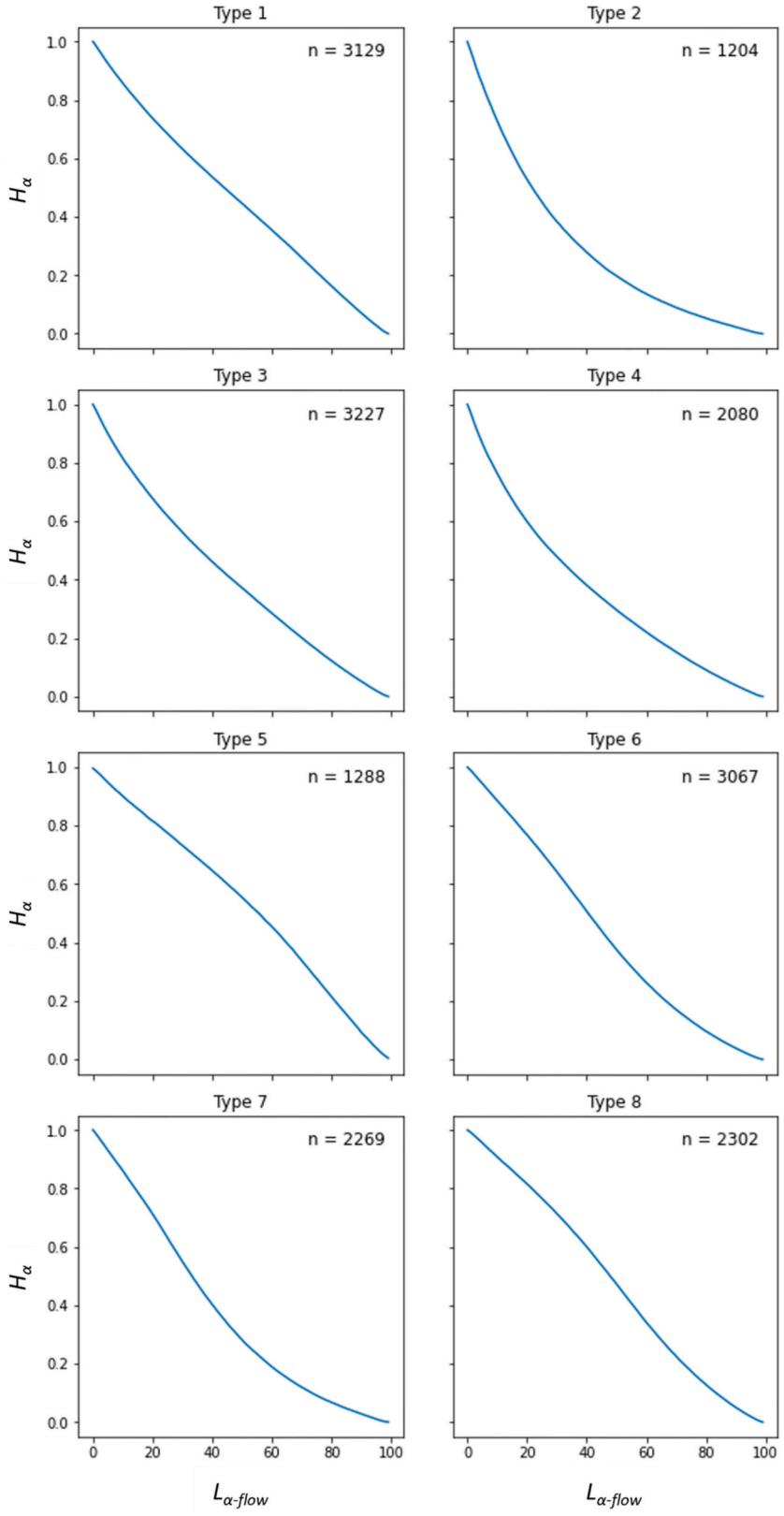

A-1: Using the K-Means algorithm it was possible to derive the eight most common path type profiles (data is normalized). The variable n is the number of samples in each path type profile.

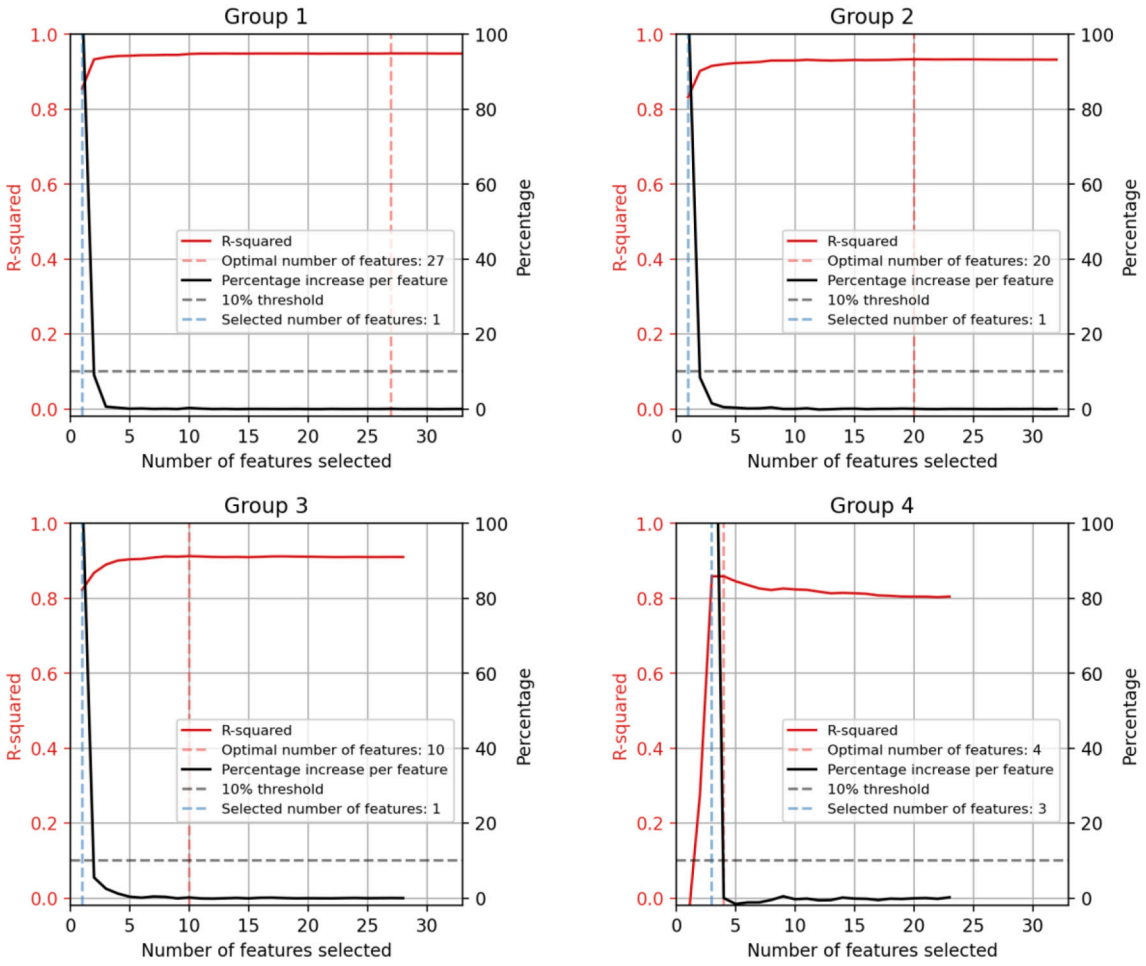

A-2: Four plots showing the R^2 value for a given number of input features for each group. These plots show us that it is not necessary to use all 33 features as input in the model to get a decent accuracy. The red dashed lines show the optimal number of features to achieve the highest possible accuracy. However, almost equally good accuracy is often achieved with much fewer features. Using a threshold of 10% (black dashed line) we can find the acceptable number of selected features (blue dashed line).

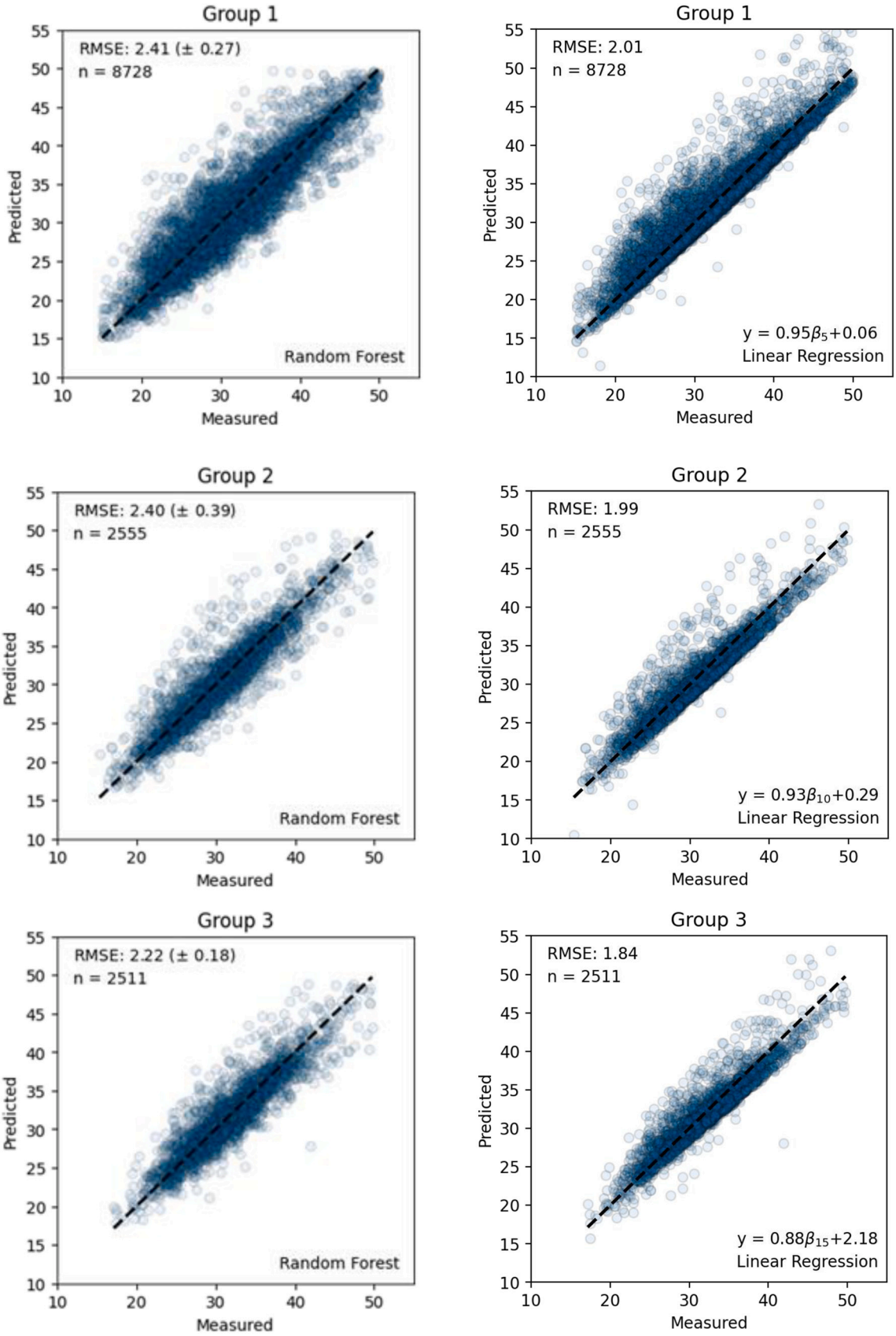

A-3: Scatter plots showing the predicted α-angles vs measured α-angles from the RF regressor for each subgroup using only the most informative features as input (Table 7). N and RMSE are shown in the upper left corner.

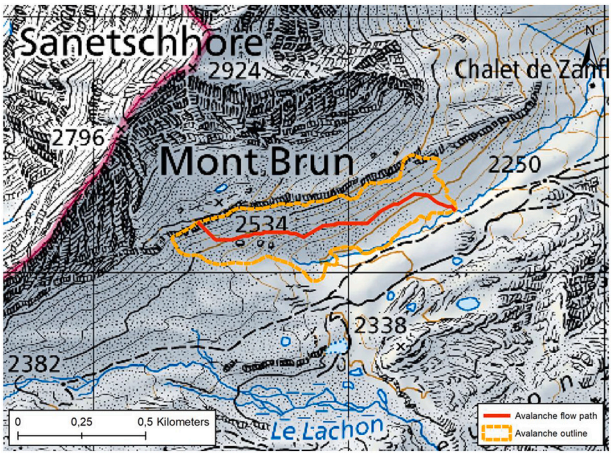

A-4: The definition of α-angle proved to not always be correct when using an automated workflow. The figure provides an example of where the flow-line from the highest point to the lowest point does not make sense. The black arrow on the red centerline marks the direction from the highest point to the lowermost point.

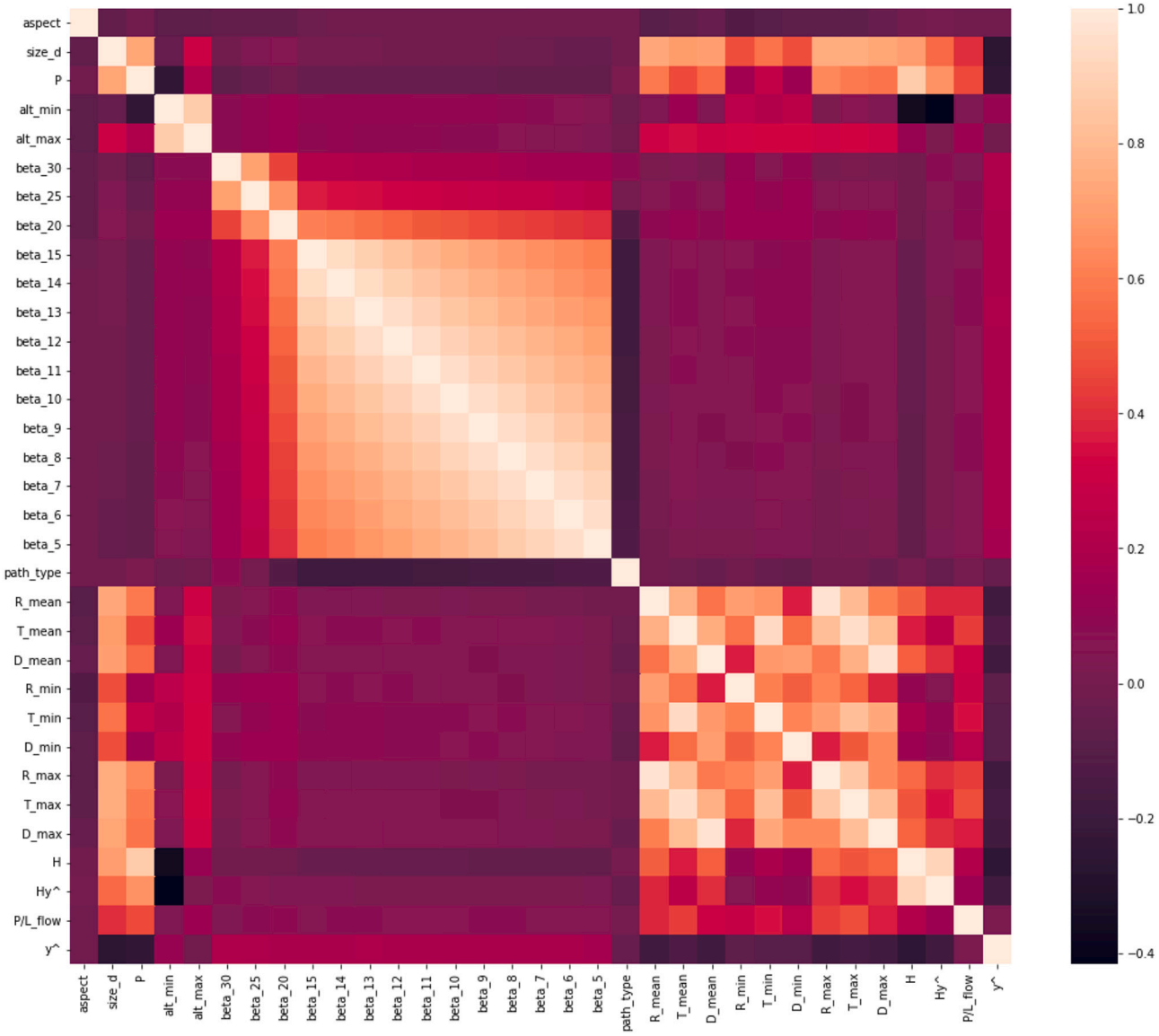

A-5: A correlation matrix showing the correlation between all factors used in the RF analysis. It clearly illustrates the correlation between the different β-angles.

References

Adjel, G., 1995. Methodes statistiques pour la determination de la distance d'arret maximale des avalanches. La Houille Blanche 7, 100–104.

American Avalanche Association, 2016. Snow, Weather and Avalanches: Observation Guidlines for Avalanche Programs in the United States (SWAG). American Avalanche Association, pp. 1–104.

Bakkehoi, S., Domaas, U., Lied, K., 1983. Calculation of Snow Avalanche Runout Distance. Ann. Glaciol. 4 https://doi.org/10.1017/S0260305500005188.

Bartelt, P., Bühler, Y., Christen, M., Deubelbeiss, Y., Salz, M., Schneider, M., Schumacher, L., 2013. RAMMS: Rapid Mass Movement Simulation: A Numerical Model for Snow Avalanches in Research and Practice. WSL Institute for Snow and Avalanche Research SLF.

Breiman, L., Friedman, J.H., Olshen, R., Stone, C.J., 1984. Classification and Regression Trees.

Bühler, Y., Kumar, S., Veitinger, J., Christen, M., Stoffel, A., Snehmani., 2013. Automated identification of potential snow avalanche release areas based on digital elevation models. Nat. Hazards Earth Syst. Sci. 13 (5), 1321–1335. https://doi.org/10.5194/nhess-13-1321-2013.

Bühler, Y., von Rickenbach, D., Stoffel, A., Margreth, S., Stoffel, L., Christen, M., 2018. Automated snow avalanche release area delineation-validation of existing algorithms and proposition of a new object-based approach for large-scale hazard indication mapping. Nat. Hazards Earth Syst. Sci. 18 (12), 3235–3251. https://doi.org/10.5194/nhess-18-3235-2018.

Bühler, Y., Hafner, E.D., Zweifel, B., Zesiger, M., Heisig, H., 2019. Alpine hazard assessment Uzbekistan View project UASs for snow depth mapping in alpine terrain View project where are the avalanches? Rapid SPOT6 satellite data acquisition to map an extreme avalanche period over the Swiss Alps. Cryosphere 13, 3225–3238. https://doi.org/10.5194/tc-13-3225-2019.

Canadian Avalanche Association, 2016. Observation Guidelines and Recording Standards for Weather, Snowpack and Avalanches. Canadian Avalanche Association, pp. 1–77.

Christen, M., Kowalski, J., Bartelt, P., 2010. RAMMS: Numerical simulation of dense snow avalanches in three-dimensional terrain. Cold Reg. Sci. Technol. 63 (1–2), 1–14. https://doi.org/10.1016/j.coldregions.2010.04.005.

Darst, B., Malecki, K., Engelman, C., 2018. Using recursive feature elimination in random forest to account for correlated variables in high dimensional data. BMC Genet. 19 (1), 1–6. https://doi.org/10.1186/s12863-018-0633-8.

Eckerstorfer, M., Bühler, Y., Frauenfelder, R., Malnes, E., 2016. Remote sensing of snow avalanches: recent advances, potential, and limitations. Cold Reg. Sci. Technol. 121 (November), 126–140. https://doi.org/10.1016/j.coldregions.2015.11.001.

Eckerstorfer, M., Malnes, E., Müller, K., 2017. A complete snow avalanche activity record from a Norwegian forecasting region using Sentinel-1 satellite-radar data. Cold Reg. Sci. Technol. 144 (December 2016), 39–51. https://doi.org/10.1016/j.coldregions.2017.08.004.

Eckerstorfer, M., Vickers, H., Malnes, E., Grahn, J., 2019. Near-Real Time Automatic Snow Avalanche activity monitoring System using Sentinel-1 SAR Data in Norway. Remote Sens. 11 (23) https://doi.org/10.3390/rs11232863.

Eckert, N., Parent, E., Naaim, M., Richard, D., 2008. Bayesian stochastic modelling for avalanche predetermination: from a general system framework to return period computations. Stoch. Env. Res. Risk A. 22 (2), 185–206. https://doi.org/10.1007/s00477-007-0107-4.

Gauer, P., Kronholm, K., Lied, K., Kristensen, K., Bakkehøi, S., 2010. Can we learn more from the data underlying the statistical α–β model with respect to the dynamical behavior of avalanches? Cold Reg. Sci. Technol. 62 (1), 42–54. https://doi.org/10.1016/j.coldregions.2010.02.001.

Gaume, J., van Herwijnen, A., Gast, T., Teran, J., Jiang, C., 2019. Investigating the release and flow of snow avalanches at the slope-scale using a unified model based on the material point method. Cold Reg. Sci. Technol. 168, 102847 https://doi.org/10.1016/j.coldregions.2019.102847.

Geron, A., 2022. Hands-on Machine Learning with Scikit-Learn, Keras, and TensorFlow, 3rd edition. O'Reilley Media.

Guyon, I., Weston, J., Barnhill, S., Vapnik, V., 2002. Gene selection for cancer classification using support vector machines. Mach. Learn. 46 (1), 389–422.

Hafner, E., Bühler, Y., 2019. SPOT6 Avalanche outlines 24 January 2018. Envidat. https://doi.org/10.16904/envidat.77.

Hafner, E.D., Techel, F., Leinss, S., Bühler, Y., 2021. Mapping avalanches with satellites – evaluation of performance and completeness. Cryosphere 15 (2), 983–1004. https://doi.org/10.5194/tc-15-983-2021.

Håland, G., Orset, K.I., Frekhaug, M.H., Norem, H., 2015. Sammenligning av modelleringsverktøy for norske snøskred.

Harvey, S., Schmudlach, G., Bühler, Y., Dürr, L., Stoffel, A., Christen, M., 2018. Avalanche Terrain Maps for Backcountry Skiing in Switzerland. International Snow Science Workshop Proceedings, Innsbruck, Austria, pp. 1625–1631.

Heim, A., 1932. Bergsturz und Menschenleben. Fretz Und Wasmuth, Zürich.

James, G., Witten, D., Hastie, T., Tibshirani, R., 2013. An Introduction to Statistical Learning, 103. Springer New York. https://doi.org/10.1007/978-1-4614-7138-7.

Jones, A.S.T., Jamieson, B., 2004. Statistical avalanche-runout estimation for short slopes in Canada. Ann. Glaciol. 38, 363–372. https://doi.org/10.3189/172756404781814960.

Keylock, C., 2005. An alternative form for the statistical distribution of extreme avalanche runout distances. Cold Reg. Sci. Technol. 42 (3), 185–193. https://doi.org/10.1016/j.coldregions.2005.01.004.

Kuhn, M., Johnson, K., 2013. Applied Predictive Modeling. Springer New York. https://doi.org/10.1007/978-1-4614-6849-3.

Larsen, H.T., Hendrikx, J., Slåtten, M.S., Engeset, R., v., 2020. Developing nationwide avalanche terrain maps for Norway. Nat. Hazards 103 (3). https://doi.org/10.1007/s11069-020-04104-7.

Li, X., Sovilla, B., Jiang, C., Gaume, J., 2021. Three-dimensional and real-scale modeling of flow regimes in dense snow avalanches. Landslides 18 (10), 3393–3406. https://doi.org/10.1007/s10346-021-01692-8.

Lied, K., Bakkehøi, S., 1980. Empirical calculations of snow avalanche run-out distances based on topographic parameters. J. Glaciol. 26 (94), 165–177.

Liu, Y., Wang, Y., Zhang, J., 2012. New Machine Learning Algorithm: Random Forest. https://doi.org/10.1007/978-3-642-34062-8_32.

Macqueen, J., 1967. Some methods for classification and analysis of multivariate observations. In: Proceedings of the Fifth Berkeley Symposium on Mathematical Statistics and Probability, 1(14), pp. 281–297.

Malnes, E., Eckerstorfer, M., Vickers, H., 2015. First Sentinel-1 detections of avalanche debris. Cryosphere Discuss. 9 (2), 1943–1963. https://doi.org/10.5194/tcd-9-1943-2015.

McClung, D.M., 2022. The scale effect in extreme snow avalanche runout distance. Can. Geotech. J. 59 (5), 625–630. https://doi.org/10.1139/cgj-2021-0146.

McClung, D., Lied, K., 1987. Statistical and geometrical definition of snow avalanche runout. Cold Reg. Sci. Technol. 13 (2), 107–119. https://doi.org/10.1016/0165-232X(87)90049-8.

McKittrick, L.R., Brown, R.L., 1993. A statistical model for maximum avalanche run-out distances in Southwest Montana. Ann. Glaciol. 18, 295–299. https://doi.org/10.3189/S0260305500011678.

Mergili, M., Fischer, J.-T., Krenn, J., Pudasaini, S.P., 2017. r.avaflow v1, an advanced open-source computational framework for the propagation and interaction of two-phase mass flows. Geosci. Model Dev. 10, 553–569. https://doi.org/10.5194/gmd-10-553-2017.

Mohri, M., Rostamizadeh, A., Talwalkar, A., 2018. Foundations of Machine Learning. MIT press.

Oller, P., Baeza, C., Furdada, G., 2021. Empirical α – β runout modelling of snow avalanches in the Catalan Pyrenees. J. Glaciol. 67 (266), 1043–1054. https://doi.org/10.1017/jog.2021.50.

Pedregosa, F., Michel, V., Grisel, O., Blondel, M., Prettenhofer, P., Weiss, R., Vanderplas, J., Cournapeau, D., Pedregosa, F., Varoquaux, G., Gramfort, A., Thirion, B., Grisel, O., Dubourg, V., Passos, A., Brucher, M., Perrot, M., Duchesnay, É., 2011. Scikit-learn: Machine Learning in Python. J. Mach. Learn. Res. 12, 2825–2830. http://scikit-learn.sourceforge.net.

Perla, R.I., Martinelli, M., 1976. Avalanche Handbook, vol. No. 489. US Dept Agric. Forest Service, Fort Collins, Colorado.

Rudolf-Miklau, F., Skolaut, C., Sauermoser, S., 2015. Avalanche Hazard Assessment and Planning of Protection Measures, in: The Technical Avalanche Protection Handbook. Ernst & Sohn, pp. 91–126. https://doi.org/10.1002/9783433603840.ch04.

Salm, B., 1972. Grundlagen des Lawinenverbaues. Bündnerwald 9, 67–81.

Scheidegger, A.E., 1973. On the prediction of the reach and velocity of catastrophic landslides. Rock Mech. 5 (4), 231–236.

Schweizer, J., Jamieson, B., Schneebeli, M., 2003. Snow avalanche formation. Rev. Geophys. 41 (4).

Swisstopo., 2018. swissALTI3D - Das hoch aufgelöste Terrainmodell der Schweiz. Swiss Federal Office of Topography Swisstopo, Berne, Switzerland.

Toft, H., 2022. GitHub Repository. Date Accessed: 03/01/2021. https://github.com/hvtola/master_thesis.

Volk, G., Kleemayr, K., 1999. ELBA–Ein GIS-gekoppeltes Lawinensimulationsmodell–Anwendungen und Perspektiven. Österreich. Zeitschr. Für Vermessung Geoinform. 2 (3).

Zweifel, B., Lucas, C., Hafner, E., Techel, F., Marty, C., Stucki, T., 2019. Schnee und Lawinen in den Schweizer Alpen, p. 86.

Bühler, Y., Bebi, P., Christen, M., Margreth, S., Stoffel, L., Stoffel, A., Marty, C., Schmucki, G., Caviezel, A., Kühne, R., Wohlwend, S., Bartelt, P., 2022. Automated avalanche hazard indication mapping on a statewide scale. Nat. Hazards Earth Syst. Sci. 22, 1825–1843. https://doi.org/10.5194/nhess-22-1825-2022.